JOURNAL OF GUIDANCE, CONTROL, AND DYNAMICS
Vol. 36, No. 1, January–February 2013

Orbit Boosting Maneuvers for Two-Craft Coulomb Formations

Hanspeter Schaub* and Lee E. Z. Jasper†
University of Colorado, Boulder, Colorado 80309

DOI: 10.2514/1.57479

This paper investigates the effectiveness of using active electrostatic charging to perform orbit altitude adjustments of a nominally circular orbit. Coulomb forces are employed to gently pull a charged object, such as space debris or a satellite being repositioned, in the along-track direction. In contrast to prior work, this study uses an enhanced position-dependent electrostatic force model. The charge at a fixed absolute potential is a function of separation distance, size, and charge of the neighboring object. The pulling configuration at a given voltage is shown to provide larger electrostatic forces over a pushing configuration. Further, the pulling configuration provides relative dynamics that are easier to stabilize. Variational equations are employed to estimate the resulting semimajor axis changes. Numerical sweeps are performed illustrating that kilovolt levels of potential are sufficient to achieve kilometer-level radius changes per orbit for geosynchronous orbit regimes. A key new insight is that, with a linear mass to effective radius scaling of the tugged object, a critical mass always exists beyond which the increased capacitance dominates over the mass increase. As a result, using the electrostatic tractor on a multiton geosynchronous orbit object can become easier if the object is larger than this critical mass.

I. Introduction

CLOSE-PROXIMITY spacecraft operations on the order of dozens of meters are challenging endeavors in that frequent orbit corrections are required to compensate for the orbital perturbations, and the close proximity makes the thruster exhaust plume impingement issues more severe. Several methods of performing propellantless relative motion control are being explored using electrostatic [1–4] or electromagnetic forces [5–8]. Lorentz-augmented orbits consider controlling the spacecraft inertial, not relative, motion using a highly charged vehicle flying in the planets magnetic field to create small Lorentz forces [9–11]. All such concepts have the significant advantage that electrical energy is primarily employed to achieve spacecraft actuation. This paper investigates doing semimajor axis orbit corrections while a tug vehicle is electrostatically tethered to a second object.

The electrostatic (Coulomb) spacecraft concept has led to a broad set of research. For example, virtual Coulomb structures consider natural relative equilibria of the charged relative motion dynamics [12–16], virtual Coulomb tethers explore replacing a physical tether with an electrostatic force between two end objects [17–20], and general cluster control algorithms are being investigated for swarms of charged satellites [21–25]. The Coulomb actuation for space applications is exciting because it can be achieved using only watt levels of electrical power for geostationary applications with I_{sp} fuel-efficiency values ranging as high as 10^9–10^{12} s [12]. Thus, for two-vehicle orbit boosting maneuvers, the electrostatic relative motion control during the orbit correction does not impact the overall orbit correction fuel budget.

Spacecraft charging occurs naturally due to the interaction with the local space environment and can reach tens of kilovolts during Earth-shaded segments of geosynchronous orbits (GEOs) as demonstrated with the ATS-6 data [26,27]. The Coulomb formation-flying (CFF) research investigates charged relative motion subject to actively controlled spacecraft potentials on the order of tens of kilovolts. To maintain a desired spacecraft potential or charge level over time, continuous charge emission is required to shift the natural charge equilibrium to a desired value [1,12].

This prior CFF research considers the use of electrostatic forces to directly control the relative motion of two or more vehicles. However, an open question that remains is how orbit correction maneuvers are performed if the Coulomb spacecraft cluster elements are not physically interconnected. For example, Natarajan et al. examine the feedback stabilization of two-craft charged equilibrium configurations in orbit radial alignment [17,20]. However, the goal of such a hybrid charge or thruster control solution is to stabilize the relative motion about a relative motion equilibrium. The center of mass of such a two-craft system is free to drift with orbital perturbations. As with nonfractionated spacecraft, there is a need to periodically adjust the orbit to maintain particular mission-sensing requirements. Although the electrostatic actuation is achievable with only watt levels of electrical power [1], the resulting forces are still very small, on the order of milli- to micronewton level. Thus, any orbit corrections of an electrostatic cluster will require 1) that the orbit correction thrust level be on the order of the electrostatic force level, or 2) that all individual components have thrusters to perform their own inertial thruster. The latter case may not be practical for many scenarios. The focus of this paper is to investigate the first scenario, in which only one component is performing inertial thrusting to change the cluster center-of-mass motion. In fractionated spacecraft concepts, such as the proposed F6 fractionated spacecraft program [28], the Coulomb spacecraft assume such unique mission roles.

An interesting application of performing orbit corrections while electrostatically interacting with a secondary spacecraft is discussed by Schaub and Moorer in [29]. Here, the Geosynchronous Larger Debris Reorbiter concept, also referred to as $GLiDeR^{TM}$, is presented where electrostatic forces are employed to tug large space debris into a disposal orbit, as illustrated in Fig. 1. The absolute potential of the debris is raised by receiving the charge emission of the tug. The tug controls its own potential to create a desired electrostatic tractor force and employs thrusting to accelerate the two-body system to a new orbit altitude, while holding a nominally constant separation distance. This charging in a space environment occurs over a fraction of a second, essentially instantaneous for the maneuver times that are on the order of orbit periods (i.e., days at GEO). Reference [29] employs a simple point-charge model of the charged bodies and does not consider specific GEO spacecraft size-to-mass relationships. Enhanced electrostatic force modeling is employed in the current study, which accounts for position-dependent capacitance models of neighboring charged bodies. Using the spacecraft potential as a fundamental control variable instead of charge, the amount of charge

Presented as Paper AAS 11-498 at the AAS/AIAA Astrodynamics Specialist Conference, Girdwood, Alaska, 31 July 2011–4 August 2011; received 28 December 2011; revision received 11 June 2012; accepted for publication 11 June 2012; published online 25 December 2012.

*Associate Professor, H. Joseph Smead Fellow, Aerospace Engineering Sciences Department. Associate Fellow AIAA.

†Graduate Research Assistant, Aerospace Engineering Sciences Department. Member AIAA.

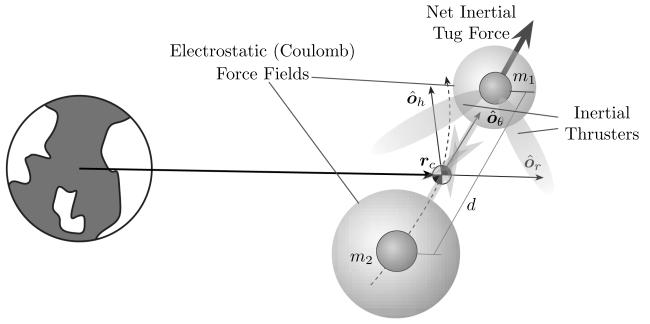

Fig. 1 Along-track aligned orbit correction of a charged two-vehicle configuration.

that is stored on an object is influenced by the presence of additional charged objects. Of interest is how this charge-to-voltage relationship impacts the ability to move large space objects. Although larger GEO spacecraft have more mass, upward of 5 t, the larger size means the craft can also store more charge with its increased capacitance.

Only circular-to-circular orbit corrections are considered where the orbit semimajor axis (SMA) is changed through long-term, small inertial thrusting in the along-track direction. Inertial thrusters employ a momentum exchange to produce a force relative to an inertial frame. In contrast, the Coulomb force is an interspacecraft force and is labeled thus a relative force that cannot change the two-body system inertial motion. SMA corrections are best performed if an along-track thrust is applied. However, this leads to two possible tug scenarios in which the second object is either pushed or pulled. This study investigates how the pushing or pulling configuration impacts the resulting performance, relative motion stability, and robustness to electrostatic tractor failure. Further, moving both fully and partially fueled large GEO spacecraft are considered, as well as small daughter sensor vehicles. These scenarios cover general repositioning of both large and small GEO satellites, as well as moving large space debris.

II. Potential-Based Electrostatic Tug Force Evaluation

A. Position-Dependent Capacitance

The electrostatic force between two point charges q_1 and q_2 separated by a distance d in a vacuum is given by

$$F_c = k_c \frac{q_1 q_2}{d^2} \tag{1}$$

where $k_c = 8.99 \times 10^9\ Nm^2/\mathrm{C}^2$ is the Coulomb constant. The vast majority of CFF research considers the dynamics and control of point charges. This equation also holds if finite spheres are considered. However, the correct potential-to-charge (i.e., capacitance) relationship must be employed. If the separation distances are large, then the voltage/charge relationship can be approximated through the isolated-sphere model [12]

$$V = k_c \frac{q}{r} \tag{2}$$

where V is the sphere potential, q is the net charge on the surface, and r is the sphere radius. This charge-to-voltage relationship changes if closely neighboring spheres are present. As experimentally demonstrated for the CFF application by Seubert and Schaub [30], the presence of another object with nonzero potential fundamentally changes the charge-to-voltage relationship. In this study, a scenario is considered in which the vehicle's absolute potential is held fixed through active charging. This charging can occur through individual active charge control of each vehicle or through indirect charging, as with the electrostatic space debris tug concept [29]. Of interest is the strength of the resulting electrostatic interaction between two finite spheres of radii r_1 and r_2, respectively, as illustrated in Fig. 2. Although this work uses spheres throughout the analytical study, [31] discusses how well general shapes can be approximated through an effective sphere if the separation distances are larger than 2–3 craft radii.

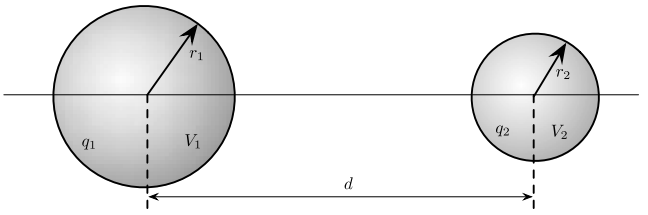

Fig. 2 Illustration of two close-proximity charged spheres.

Assume the two conducting spheres have each a potential V_1 and V_2. The potential on sphere 1 is computed as the sum of the self-capacitance relationship in Eq. (2) and the potential due to the second body of charge q_2 as [32]

$$\begin{bmatrix} V_1 \\ V_2 \end{bmatrix} = k_c \begin{bmatrix} \frac{1}{r_1} & \frac{1}{d} \\ \frac{1}{d} & \frac{1}{r_2} \end{bmatrix} \begin{bmatrix} q_1 \\ q_2 \end{bmatrix} \tag{3}$$

Note that the potentials in this paper are all assumed to be taken relative to a zero potential at infinity. Even with spheres held at fixed potentials, the charge distribution can be nonhomogenous if the two spheres are very close to each other [33]. However, this induced-charge effect is negligible if the separation distance is more than three craft radii, as is assumed in this study. Inverting Eq. (3) for the charges yields

$$\begin{bmatrix} q_1 \\ q_2 \end{bmatrix} = \underbrace{\frac{d}{k_c(d^2 - r_1 r_2)} \begin{bmatrix} r_1 d & -r_1 r_2 \\ -r_1 r_2 & r_2 d \end{bmatrix}}_{[C(d)]} \begin{bmatrix} V_1 \\ V_2 \end{bmatrix} \tag{4}$$

The 2×2 matrix $[C(d)]$ is the capacitance matrix for this two-sphere system, which is a function of the separation distances. Note that, depending on the signs of the potentials, the amount of charge stored on each sphere can be either increased or decreased in contrast to the isolated-sphere charge/voltage relationship in Eq. (2).

Substituting the charges q_1 and q_2 in Eq. (4) into the electrostatic force expression in Eq. (1) yields the electrostatic tractor force magnitude used in this study:

$$F_c = \frac{r_1 r_2 (V_1 r_1 - V_2 d)(V_1 d - V_2 r_2)}{k_c (d^2 - r_1 r_2)^2} \tag{5}$$

The sign of F_c is chosen such that the positive value indicates an attractive force, and a negative value is for a pushing scenario. This position-dependent capacitance relationship has been experimentally demonstrated using the one-dimensional electrostatic charged relative motion test bed in 30. This paper investigates how the two-craft system can perform orbit-raising maneuvers while only one spacecraft is performing continuous inertial thrusting. The nominal inertial thrust magnitude cannot exceed the magnitude of this electrostatic tractor force F_c without causing the spacecraft formation to shear apart. Thus, the orbit-raising performance is coupled to the potentials and capacitance of the two-craft system.

In this study, the separation distance d is assumed to be held constant using a dedicated relative motion feedback control loop. Thus, stationkeeping has its own challenges due to the nonlinear nature of the electrostatic tractor. Reference [34] discusses a nonlinear relative motion control strategy to achieve such stationkeeping while electrostatically tugging a second object. The force in Eq. (5) is used as a nominal debris actuation to estimate the open-loop reorbiting performance.

B. Space Weather Impact

These charge-to-voltage relationships assume that the space weather impact is negligible. This section briefly discusses why this is a reasonable assumption for nominal GEO operators. As discussed by Denton et. al. [35], the nominal space weather can vary across the geosynchronous orbit region as different local time locations are

considered, as well as due to solar disturbances to Earth's magnetic field expressed through the K_p index. If the spacecraft potential V is small compared with the plasma temperature T_e (i.e., $eV < kT_e$), then the approximate potential relationship about a finite sphere with a surface potential V_s and radius r in this plasma is [36,37]

$$V(d) = V_s \frac{r}{d} e^{-(d-r)/\lambda_D} \tag{6}$$

where d is the center-to-center separation distance, and λ_D is the Debye–Hückel length. Reference [35] studies the nominal plasma temperatures and densities for a 10 year period. The results indicate that the minimum debye lengths across a GEO orbit range between 180 and 200 m, depending on the solar activity and the local time. This charge-shielding distance is much larger than the small separation distances of 10–25 m considered in this study. Further, because relatively large potentials are being considered with respect to the GEO plasma energy levels, the small relative potential approximation of Eq. (6) only yields conservative worst-case estimates of the amount of charge shielding that would be experienced. The large potentials result in a weakening of the charge shielding, as discussed in [38], and effective debye lengths that are 2–3 times larger. Thus, the omission of the space weather influence on performing electrostatic orbit corrections is justifiable even for harsh GEO space weather conditions with tens of meter debye lengths. Future work could consider space weather extremes that might be encountered and how this impacts the nontrivial electrostatic force-and-vehicle capacitance relationship.

III. Pulling and Pushing Configuration Considerations

A. Electrostatic Force Considerations

To perform low-thrust SMA corrections, the most efficient thrusting solution is in the current along-track direction [39]. For a two-craft cluster, this yields two possible scenarios to perform the SMA changes, in which the thrusting vehicle is either in the lead tugging or trailing and pushing the second vehicle. The pulling or tugging configuration requires an attractive electrostatic force between the two bodies, and thus the potentials must satisfy the condition $V_1 V_2 < 0$. The pushing scenario requires a repulsive force with $V_1 V_2 > 0$.

Studying the electrostatic force expression in Eq. (5) with fixed sphere surface potentials V_1 and V_2, it is evident that having potentials with opposite signs causes an increase in the electrostatic force. The reason for this force increase is visualized in Fig. 3. Although sphere 1 is holding a fixed absolute potential $V_1(0)$ on its surface, the amount of charge q_1 stored on the sphere to achieve this potential is dependent on the potential fields of neighboring objects. For example, assume that the conducting sphere 1 has no potential control active. Because of the presence of a second object with charge q_2, sphere 1 will assume the potential $V_2(d)$ that the second sphere yields at a separation distance d. Consider the pulling scenario 1 where $V_1 V_2 < 0$, shown in Fig. 3a. Without loss of generality, assume V_2 is positive. Here, body 1 must accumulate negative charge just to bring its potential down to zero. To achieve the desired $V_1(0) < 0$ value, additional negative charge is required. In contrast, Fig. 3b illustrates the pushing scenario 2 in which both spheres have the same charge polarity. Here, the first sphere will already have a negative potential without any additional charge accumulation. Thus, less negative charge is required to reach the desired $V_1(0)$ surface potential. As a result, the pushing configuration at the same absolute voltage magnitude leads to a smaller electrostatic actuation, whereas the pulling configurations yield a stronger actuation and orbit correction performance.

The impact of this position-dependent capacitance on the resulting electrostatic force magnitude is further illustrated in Fig. 4. Three primary cases are considered, each with two spheres having 2 m radii and 20 kV potential magnitudes. The solid line computes the electrostatic forces assuming each sphere is isolated with the charge computed using Eq. (2). The dashed-dotted line considers an electrostatic attractive force scenario where $V_1 V_2 < 0$ and uses Eq. (4) to evaluate the charges. The dashed line illustrates the force magnitude for a repulsive scenario with $V_1 V_2 > 0$ also evaluated using Eq. (4). The smallest feasible separation distance in this scenario is 4 m, where the sphere surfaces would be touching. At the minimum separation, the attractive force scenario yields an electrostatic force 4 times larger for the same potential in comparison with the isolated-sphere model. The repulsive scenario yields a force that is about half. Naturally, electrostatic orbit corrections will not occur with the objects almost touching each other. Instead, CFF considers center-to-center separation distances of 10–25 m. As

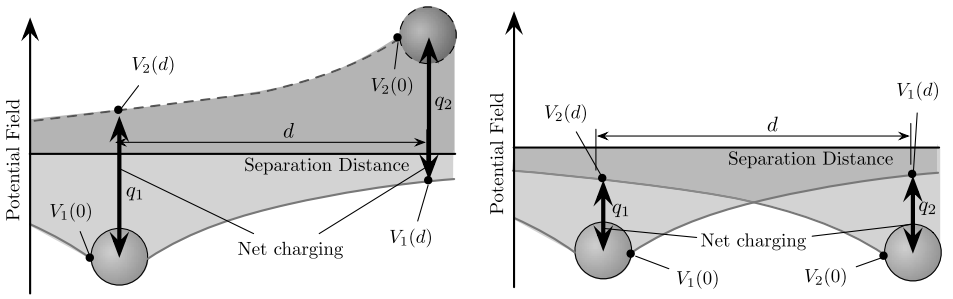

a) Scenario 1: pulling **b) Scenario 2: pushing**

Fig. 3 Illustration of neighboring potential impact on local capacitance and net charging.

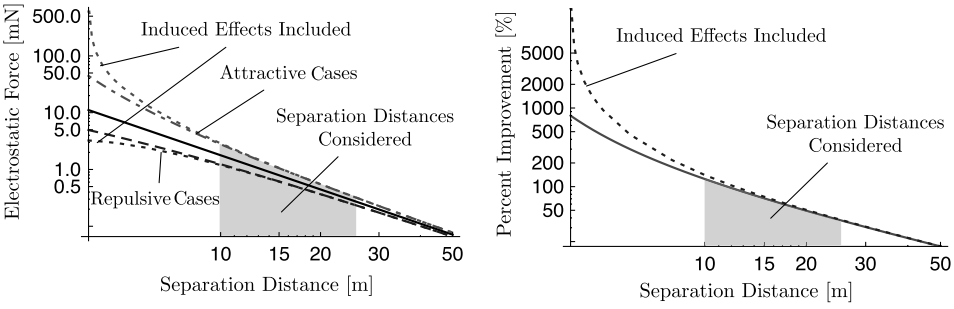

a) Force magnitude comparison **b) Ratio of attractive vs. repulsive forces**

Fig. 4 Electrostatic force illustration for two 2-m-radius spheres at 20 kV.

illustrated in Fig. 4b, for separation distances ranging 10–25 m (shaded region in Fig. 4), the attractive electrostatic forces are 50–100% larger compared with the repulsive electrostatic force magnitude for equivalent potential magnitudes. Thus, from an electrostatic force evaluation perspective, the tugging scenario with attractive electrostatic forces yields significant performance improvements for performing electrostatic orbit corrections.

Figure 4 also shows the expected electrostatic force between two spheres if induced-charge effects are included using the iterative solution provided by Soules [33]. Here, the nonhomogenous charge distribution on two conductive surfaces causes an increase in the attractive force. This results in a strengthening of the electrostatic attraction over a very short distance (less than 3–4 craft radii) and additional weakening of the repulsive force. This further favors the pulling orbit correction configuration. Further, this example illustrates that, although position-dependent capacitance effects are significant for the separation distances considered, the induced effects are negligible for this study.

B. Relative Orientation Stability Considerations

Besides the electrostatic force argument for a given voltage level, another argument favoring the pulling configuration for orbit corrections is the resulting relative dynamics. Even if the separation distance between the satellite is being held fixed with a feedback control strategy, the relative orientation of the two satellites is open-loop unstable. The two configurations considered are illustrated in Fig. 5. Considering $\ddot{x} > 0$ to be a constant acceleration, and $\dot{x}(t) > 0$, then the linear angular departure motion θ differential equations are either

$$\text{Pulling:}\quad L\ddot{\theta} + \dot{x}\,\dot{\theta} + \ddot{x}\theta = 0 \tag{7a}$$

$$\text{Pushing:}\quad L\ddot{\theta} - \dot{x}\,\dot{\theta} - \ddot{x}\theta = 0 \tag{7b}$$

The positive pushing acceleration causes a negative stiffness and thus unstable relative orientation oscillations. In contrast, the pulling configuration leads to stable oscillations in this simple dynamic illustration example. For the electrostatic orbit correction application, it will be significantly simpler to control the relative motion with the second object if the thrusting object is in the lead pulling the other. The pulling configuration will require that the lead's exhaust plume does not impinge on the second object. This can be achieved with angled or boom-displaced thrusters, which direct the exhaust plume into free space.

C. Electrostatic Tractor Robustness Considerations

Finally, safety considerations are considered if the electrostatic tractor fails while the inertial thrusters are active. Both the thrusters and the tractor could be disengaged very quickly, in less than a second, if needed. If any component fails, the goal is to separate and achieve a safe standby configuration. The pulling configuration is preferred because the thrusters will simply cause the tug to pull away from the second object, and no immediate collision-avoidance maneuver needs to be engaged. The thrusters can be safely disengaged after detecting an electrostatic tractor failure, and the craft already have the desired separating motion. In contrast, with the pushing configuration, a failure of the electrostatic actuation will result in the thrusting accelerating the tug toward the second object, requiring an immediate avoidance maneuver.

IV. Numerical Orbit-Raising Performance Study

A. Electrostatic Semimajor Axis Changes

Orbital variational equations are used to obtain analytical predictions of the amount of semimajor axis changes Δa that are feasible for ranges of spacecraft potentials, dimensions, and mass. Let a_r and a_θ be the orbit radial and along-track disturbance accelerations. Gauss's variational equation for the SMA a is [39,40]

$$\frac{\mathrm{d}a}{\mathrm{d}t} = \frac{2a^2}{h}\left(e\,\sin f a_r + \frac{p}{r}a_\theta\right) \tag{8}$$

where h is the orbit angular momentum, p is the semilatus rectum, e is the eccentricity, f is the true anomaly, and r is the current orbit radius. For this study, the Coulomb spacecraft cluster is assumed to have a near-zero eccentricity with $e \to 0$, $r \to a$, and $p \to a$. Although the orbit correction is accomplished through a spiraling trajectory, the path can be locally approximated as a circle. For a nearly circular orbit with a vanishingly small eccentricity, the momentum is approximated through $h \approx a^2 n$, where n is the mean orbit rate. The SMA differential equation in Eq. (8) reduces to

$$\frac{\mathrm{d}a}{\mathrm{d}t} = \frac{2a_\theta}{n} \tag{9}$$

Let m_1 be the mass of the object performing the inertial thrusting, and let m_2 be the object that is electrostatically towed to a new orbit. The along-track acceleration of m_2 is given by

$$a_\theta = \frac{|F_c|}{m_2} \tag{10}$$

where the electrostatic force acting on m_2 is determined through Eq. (5). The absolute value operator is employed with F_c to account for the fact that a_θ is positive for both the pulling and pushing configurations considered. Thus, although the pulling configuration is preferred, the following development holds for both cases.

Note that the orbit correction performance is limited by the magnitude of the electrostatic tractor force F_c. The tugging vehicle with mass m_1 must thus employ the nominal thrust

$$F_1 = \frac{m_1 + m_2}{m_2}F_c \tag{11}$$

to accelerate both m_2 and itself by the same amount and thus maintain a fixed nominal separation distance. With potentials in the tens of kilovolts, the thrust levels are in the millinewton range. To study the reorbiting performance while electrostatically actuating a second object, it is sufficient to consider the acceleration a_θ in Eq. (10).

Let $P = 2\pi/n$ be the orbit period, then the SMA change per orbit due to a constant along-track acceleration a_θ is approximated through

$$\Delta a \approx \frac{\mathrm{d}a}{\mathrm{d}t}\cdot P = \frac{4\pi}{n^2}a_\theta \tag{12}$$

Substituting Eqs. (5) and (10) into Eq. (12) yields an estimate of the SMA change that can be produced over one orbit revolution:

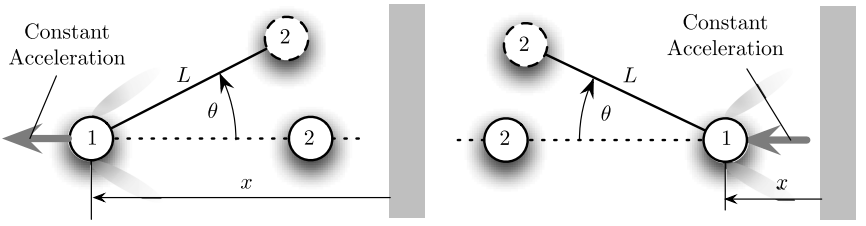

a) Pulling configuration **b) Pushing configuration**

Fig. 5 Dynamic illustration of a pushed and pulled fixed length pendulum configuration subject to a constant acceleration on object 1.

$$\Delta a \approx \frac{4\pi}{n^2}\frac{r_1 r_2 (V_1 r_1 - V_2 d)(V_1 d - V_2 r_2)}{k_c m_2 (d^2 - r_1 r_2)^2} \tag{13}$$

In contrast to the SMA change prediction provided in [29], the Δa per orbit expression in Eq. (13) explicitly accounts for the position-dependent capacitance results from neighboring charged objects. The accuracy of using this variational approach to predict these relatively small SMA changes at GEO are numerically verified in the earlier study in [29]. The SMA change performance is still inversely proportional to the mass m_2, which is being towed to a new orbit. However, in contrast to earlier work using simplifying isolated-sphere charge-to-voltage relationships, the SMA correction per orbit is now a complex relationship between separation distance d and effective spherical radii r_i of either object.

B. Case 1: Towing Large Geostationary Objects

Next, numerical sweeps are employed to illustrate the expected performance levels to apply orbit corrections to both large and small geosynchronous objects. First, let us consider the case in which both objects are similarly large objects. In this scenario, the two-body system could be a fractionated spacecraft concept in which a free-flying element contains the inertial thrusters to perform the orbit corrections, whereas the second object contains the science or communication instruments of the geostationary satellite. This scenario also depicts the electrostatic debris removal method discussed in [29]. Of interest is how well electrostatic forces can be employed to reposition another satellite or to move large defunct satellites and space debris.

In this scenario, the tugging vehicle 1 is assumed to have a spherical shape of radius r_1, whereas the second object could be a regular satellite with a general three-dimensional shape. However, Eq. (13) assumes both objects are spheres. Reference [31] provides an extensive study on how well three-dimensional shapes can be represented through effective spheres. As with gravitational fields about three-dimensional shapes, the larger the separation distance is, the more the three-dimensional electrostatic field approaches that of a sphere. Reference [31] demonstrates that, even with solar panels expanding 4–7 m from the spacecraft center, for separation distances larger than 15 m, the first-order effective sphere model deviates from the exact 3-D electrostatic models by only 10–15% at worst. For cylindrical shapes, such as used with dual-spinner satellites, the deviations over these separation distances are 5% or less.

The first-order effective sphere model requires extensive finite element-based numerical modeling of the true electrostatic field about a general shape, and then fitting the effective radius to these data. In this study, the goal is to obtain approximate SMA performance measures for a large range of bodies. Instead of using the first-order effective sphere model, this study employs the zeroth-order effective sphere model discussed in [31]. Here, the total outer surface area is estimated, and then this area is mapped to a sphere to yield an equivalent sphere radius. This simpler and faster method yields representative craft radii, which can differ by about 10% from the more complex first-order method.

Next, to use Eq. (13) to predict SMA changes, it is important that a realistic mass-to- size relationship be used. For example, a more massive satellite also tends to have a larger size and thus a larger capacitance. As a result, it is not readily apparent that a larger satellite will result in a lower SMA change performance for a given voltage level.

Approximate launch mass and satellite dimensions are obtained using a public NASA Web site[‡] discussing geostationary satellite data. Figure 6 illustrates the resulting mass to zeroth-order effective radius [31] for a range of GEO resident space objects (RSO). Here, the outer surface area of a general shape is mapped onto a sphere of equal surface area to approximate the capacitance. These data yield a mass-to-effective-radius relationship of

[‡]Data available online at http://nssdc.gsfc.nasa.gov/nmc/SpacecraftQuery.jsp [retrieved 31 October 2012].

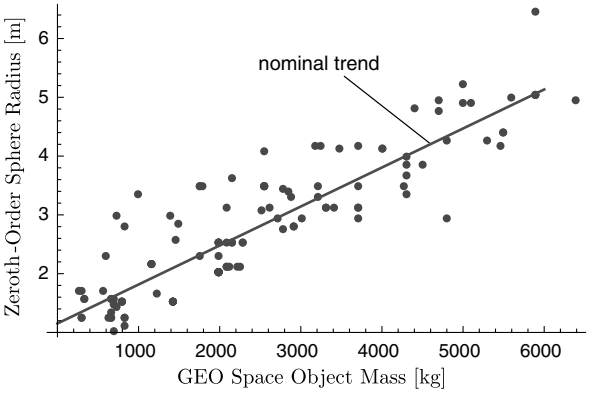

Fig. 6 Illustration of the nominal size-to-mass trend of geosynchronous RSOs.

$$r_2(m_2) = 1.152\ \text{m} + 0.00066350\frac{\text{m}}{\text{kg}}\text{m}_2 \tag{14}$$

where r_2 is in units of meters, and m_2 is in units of kilograms. Please note that this relationship of the NASA site provides the launch masses of each satellite. Thus, Eq. (14) illustrates the worst-case mass-to-area ratio one could have.

Some newer GEO satellite designs employ fuel-efficient low-thrust technologies to perform their stationkeeping. Even after years of operation, the launch mass remains a good estimate of the total spacecraft mass. On the other hand, for many older geostationary satellite designs, the fuel stored for orbit corrections is a significant fraction of the total mass. Thus, considering the electrostatic space debris removal problem, both the launch mass case and the scenario in which significant fuel mass has been used are of interest. As mass is reduced, the capacitance of the satellite remains the same, thus aiding the orbit boost performance.

1. *Semimajor Axis Changes with Initial Launch Mass.*

First, let us consider what SMA changes are feasible per geosynchronous orbit (24 h) using the Δa approximation in Eq. (13) and the GEO RSO mean mass-to-radius relationship in Eq. (14). This scenario studies a recently launched satellite needing a boost or a defunct space debris object that employed electric propulsion. The Coulomb craft with inertial thrusters is ahead of the towed Coulomb vehicle in a pulling configuration.

Figure 7 sweeps the towed mass from 500 to 5000 kg, and the voltages from 0 to 40 kV. This study assumes $V_1 = -V_2$. Four scenarios are shown with center-to-center separation distances of 25, 20, 15, and 10 m. Given the larger outer dimensions of many GEO satellites, separation distances shorter than 10 m result in significant collision risks. The Coulomb vehicle with inertial thruster is assumed to have a radius of 3 m for all numerical sweeps.

The ATS-6 mission has shown that natural charging during solar storm activities can reach 18 kV. Thus, the potentials considered here are of a similar magnitude. Studying Fig. 7b, if the towed object has a mass of 1000 kg and a separation distance of 20 m, then a 20 kV potential would result in SMA changes of about 1.9 km/day. A 10 km correction could be accomplished using a low-thrust spiraling trajectory over only 5.2 days. If a larger object of 2000 kg mass is considered, the SMA changes reduce to about 1.3 km/day. To raise GEO space debris to a 250 km disposal region, this setup would take approximately 192 days, or about six months. Dashed lines are used to illustrate these example scenarios in the figures. Please keep in mind that these performance values are approximate mean values, as the true effective radius of GEO objects can vary considerably, as shown in Fig. 6. Note that the SMA change performance does not scale with the mass of the towed object because larger objects also have a larger capacitance. Rather, the performance contours flatten significantly as the mass is increased. If very short 10 m separation distances are considered as shown in Fig. 7d, the performance curve becomes flat and even reverses direction, indicating that it is possible

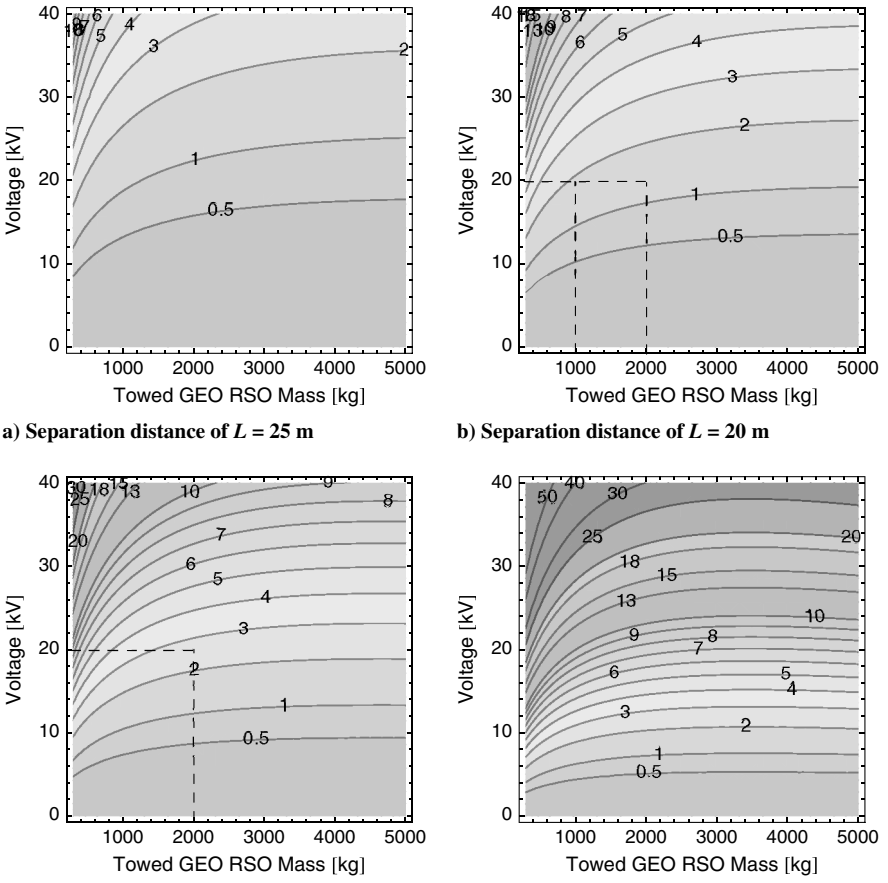

a) Separation distance of L = 25 m **b) Separation distance of L = 20 m**

c) Separation distance of L = 15 m **d) Separation distance of L = 10 m**

Fig. 7 Kilometer SMA changes per orbit period assuming an initial launch mass.

for a more massive object to yield higher SMA change performances. Thus, by controlling the objects potential, moving large space debris is feasible thanks to the larger capacitance of the large debris objects.

Shorter separation distances have a strong impact on the SMA change performance due to the near-inverse-square relationship between the electrostatic force and separation distance. At 15 m separation, the 2000 kg object results in about 2.6 km/day SMA changes. This is equivalent to a 3.2 month space debris reorbit time to a 250 km GEO disposal orbit.

2. Semimajor Axis Changes with Sixty Percent Launch Mass.

Next, let us consider a mass-to-radius relationship of the towed vehicle, which assumes the current mass is 60% of the initial launch mass. This scenario assumes that a large amount of fuel has been used for stationkeeping over its lifetime. For electrostatic orbit corrections, this increases the magnitudes of the orbit corrections as the towed vehicle retains the same capacitance, but now has less mass. For the space debris removal application, moving older GEO satellites with larger capacitance to mass ratios provides a significant performance boost.

The numerical sweeps of Fig. 7 are repeated in Fig. 8 with this new mass-to-radius relationship for separation distances of 20 and 15 m. The SMA change performance for the 2000 kg case with 20 kV increases from 1.3 to about 1.9 km/day for the 20 m separation distance scenario. This reduces the 250 km reorbit time from 192 to 132 days. Further, note that, with this small mass-to-radius ratio, the contour lines in Fig. 8 are flatter than with the larger mass and even reverse the trend at smaller masses. This illustrates that, with a given

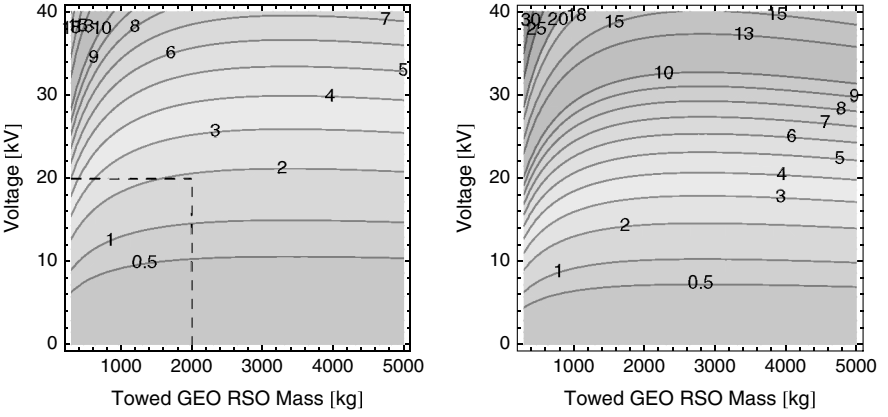

a) Separation distance of L = 20 m **b) Separation distance of L = 15 m**

Fig. 8 Kilometer SMA changes per orbit period assuming 60% of initial launch mass.

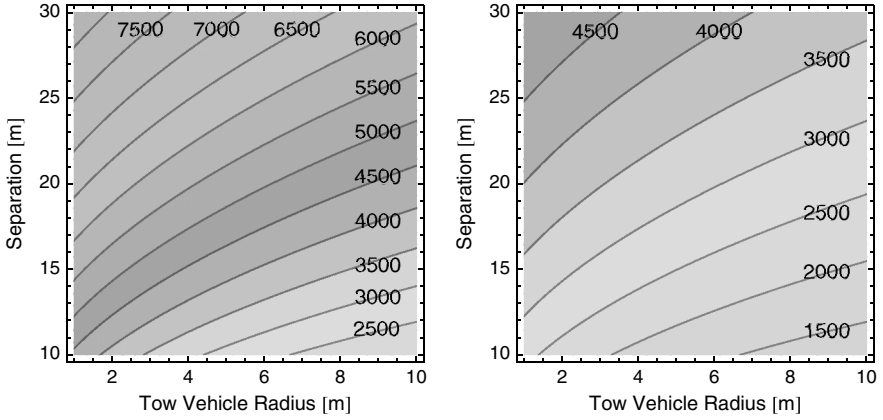

a) GEO object launch mass case **b) Case assuming 60% of GEO object launch mass**

Fig. 9 Critical mass study illustrating from what mass (units in kilograms) onward the electrostatic orbit correction becomes easier due to the increase object capacitance.

potential, moving the 2, 3, 4, or 5 ton space debris objects results in similar SMA-raising performance levels.

C. Critical Mass Study

Let us consider this reverse of SMA change effort in more detail. Assuming a linear radius-to-mass relationship of the towed vehicle

$$r_2(m_2) = a_0 + a_1 m_2 \tag{15}$$

the inflection points of the SMA changes Δa in Eq. (13) with respect to m_2 are of interest. Making the assumption $V_1 = -V_2$, the SMA correction per orbit simplifies to

$$\Delta a \approx \frac{4\pi}{n^2} \frac{r_1 r_2(m_2) V_1^2 (r_1 + d)(r_2(m_2) + d)}{k_c m_2 (d^2 - r_1 r_2)^2} \tag{16}$$

The m_2 inflection points are determined by solving

$$\frac{\partial(\Delta a)}{\partial m_2} = 0 \tag{17}$$

With the potential constraint $V_1 = -V_2$, the resulting critical masses that satisfy Eq. (17) do not depend on the vehicle potentials.

Figure 9 illustrates the critical towed vehicle masses m_2 for both launch mass and 60% launch mass cases. The center-to-center separation distances are swept from 10 to 30 m, and 1–10 m tug vehicle radii are considered. With the full launch mass, a 3 m radius tug vehicle with a 20 m separation distance has a critical tow mass of $m_2 = 6000$ kg. This means that, for vehicles more massive than this critical mass, larger changes in the SMA are feasible due to the dominating capacitance impact. If a smaller mass-to-radius relationship than having 60% of the initial launch mass is assumed, the same 3 m tug at 20 m separation has a lower critical tow mass m_2 of about 3500 kg. Further, Fig. 9 illustrates the trend that large tug radii will result in lower critical tow masses. Although the critical mass concept does not provide direct design constraints on how large the tug should be, it does provide some interesting insight. For example, if the tug radius is about 4 m and the separation distance is approximately 15 m, the critical mass is about 4500 kg. As a result, the reorbiting performance leading up to 4500 kg objects is expected to be flat and is guaranteed to improve, although by a small amount, for objects larger than 4500 kg.

D. Case 2: Towing a Small Free-Flying Sensor Object

The preceding section considered the scenario in which a large Coulomb tug pulls on a large geostationary satellite. Next, the setup is considered in which a large GEO mothercraft has a smaller daughter vehicle deployed. The separation distance between the two is controlled through electrostatic forces. The daughter vehicle could be flying 10–20 m from the mothercraft to provide local situational awareness about the mothercraft or provide images to inspect the exterior hull for damage due to space debris or micrometeorites.

At first glance, it might seem that this is a much easier scenario in which to perform orbit corrections because the large mothercraft is towing a much lighter secondary vehicle. However, due to the smaller size of the daughter vehicle, it will also provide a smaller charge

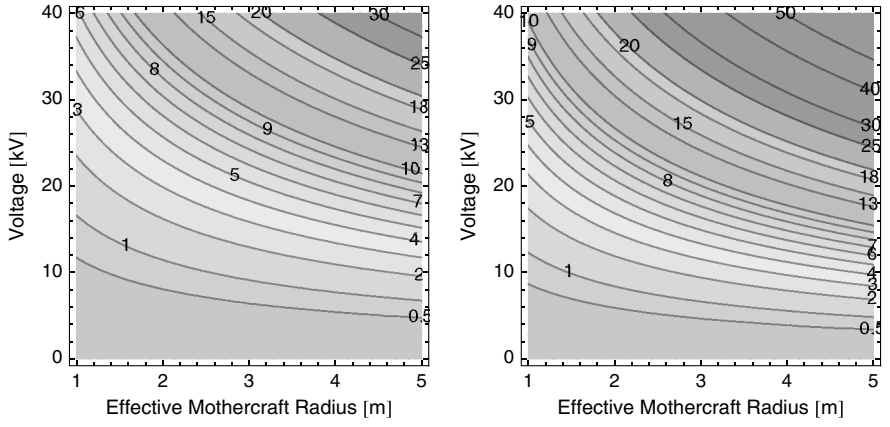

a) Separation distance of L = 20 m **b) Separation distance of L = 15 m**

Fig. 10 Mother–daughter SMA changes (in kilometers) per orbit period.

capacitance. Figure 10 illustrates the expected SMA changes per orbit (per day), assuming the daughter vehicle is a small, spherical, 100 kg vehicle with 0.5 m radius. Assuming a 20 m separation distance, an effective mothercraft radius of 3 m, and $V_1 = -V_2 =$ 20 kV, the expected SMA changes are about 4.5 km/orbit. In contrast, the SMA performance in Fig. 8a shows a performance of about 2–3 km/orbit for masses of 1000–5000 kg. Thus, the mother–daughter vehicle scenario reinforces the conclusion that lighter or heavier objects are not necessarily easier or more challenging to reorbit electrostatically.

V. Conclusions

Coulomb forces have been considered for relative motion control for over a decade. This paper discusses how to perform simple semimajor axis correction maneuvers while two free-flying spacecraft are electrostatically tethered to each other. The charge is studied using the absolute potential of each vehicle. Pulling configurations with attractive electrostatic forces are found to provide larger actuation than pushing configurations with repulsive electrostatic forces. The semimajor axis changes per orbit are analytically predicted using Gauss's variational equations. Considering the space debris removal application, numerical performance sweeps illustrate that even large, multiton debris objects can be electrostatically reorbited over a period of months. In fact, assuming a linear mass-to-radius relationship, for every separation distance and vehicle potential consideration, there is a critical mass beyond which performing orbit corrections at a given potential actually becomes easier again. Further, a mother–daughter vehicle case is considered where the daughter vehicle is small and light. Although this configuration produces larger semimajor axis changes per orbit, the increase in performance is only marginal compared with the larger object towing case due to the significantly decreased capacitance of the smaller vehicle.

Acknowledgments

We would like to thank Daniel Moorer and the Wacari Group for their support of this research and for feedback on the viability of this concept. We also thank Daniel Baker for helpful discussions on geosynchronous orbit space weather variability.

References

[1] Cover, J. H., Knauer, W., and Maurer, H. A., "Lightweight Reflecting Structures Utilizing Electrostatic Inflation," U.S. Patent 3,546,706, Oct. 1966.

[2] Schaub, H., Parker, G. G., and King, L. B., "Challenges and Prospect of Coulomb Spacecraft Formation Control," *Journal of Astronautical Sciences*, Vol. 52, Nos. 1–2, 2004, pp. 169–193.

[3] King, L. B., Parker, G. G., Deshmukh, S., and Chong, J.-H., "Study of Interspacecraft Coulomb Forces and Implications for Formation Flying," *Journal of Propulsion and Power*, Vol. 19, No. 3, 2003, pp. 497–505. doi:10.2514/2.6133

[4] Pettazzi, L., Krüger, H., and Theil, S., "Electrostatic Forces for Satellite Swarm Navigation and Reconfiguration–Final Report," European Space Research and Technology Centre (ESA), Technical Rept. Ariadna ID: 05/4107, 2006.

[5] Kong, E. M. C., and Kwon, D. W., "Electromagnetic Formation Flight for Multisatellite Arrays," *Journal of Spacecraft and Rockets*, Vol. 41, No. 4, 2004, pp. 659–666. doi:10.2514/1.2172

[6] Miller, D. W., Sedwick, R. J., Kong, E. M. C., and Schweighart, S., "Electromagnetic Formation Flight for Sparse Aperture Telescopes," *IEEE Aerospace Conference Proceedings*, Vol. 2, Big Sky, Montana, 9–16 March 2002, pp. 729–741.

[7] Ashun, U., "Dynamics and Control of Electromagnetic Satellite Formations in Low Earth Orbits," *AIAA Guidance, Navigation, and Control Conference*, AIAA Paper 2006-6590, 2006.

[8] Villani, D. D., and Landecker, P. B., "Magnetic Systems and Methods for Realizing Spacecraft Maneuvers," U.S. Patent 6,089,510, 18 July 2000.

[9] Yamakawa, H., Bando, M., Yano, K., and Tsujii, S., "Spacecraft Relative Dynamics Under the Influence of Geomagnetic Lorentz Force," *AIAA Guidance, Navigation and Control Conference*, AIAA Paper 2010-8128, 2010.

[10] Peck, M. A., Streetman, B., Saaj, C. M., and Lappas, V., "Spacecraft Formation Flying Using Lorentz Forces," *Journal of British Interplanetary Society*, Vol. 60, July 2007, pp. 263–267.

[11] Peck, M. A., "Prospects and Challenges for Lorentz-Augmented Orbits," *AIAA Guidance, Navigation and Control Conference*, AIAA Paper 2005-5995, 2005.

[12] King, L. B., Parker, G. G., Deshmukh, S., and Chong, J.-H., "Spacecraft Formation-Flying Using Inter-Vehicle Coulomb Forces," NASA Inst. for Advanced Concepts TR, Jan. 2002, http://www.niac.usra.edu.

[13] Berryman, J., and Schaub, H., "Static Equilibrium Configurations in GEO Coulomb Spacecraft Formations," *Advances in Astronautical Sciences*, Vol. 120, 2005, pp. 51–68. ; also American Astronautical Society Paper 05-104, 2005.

[14] Schaub, H., Hall, C., and Berryman, J., "Necessary Conditions for Circularly-Restricted Static Coulomb Formations," *Journal of Astronautical Sciences*, Vol. 54, Nos. 3–4, July–Dec. 2006, pp. 525–541.

[15] Berryman, J., and Schaub, H., "Analytical Charge Analysis for 2- and 3-Craft Coulomb Formations," *Journal of Guidance, Control, and Dynamics*, Vol. 30, No. 6, 2007, pp. 1701–1710. doi:10.2514/1.23785

[16] Vasavada, H., and Schaub, H., "Analytic Solutions for Equal Mass Four-Craft Static Coulomb Formation," *Journal of Astronautical Sciences*, Vol. 56, No. 1, Jan.–March 2008, pp. 17–40.

[17] Natarajan, A., Schaub, H., and Parker, G. G., "Reconfiguration of a Nadir-Pointing 2-Craft Coulomb Tether," *Journal of British Interplanetary Society*, Vol. 60, No. 6, June 2007, pp. 209–218.

[18] Natarajan, A., and Schaub, H., "Orbit-Nadir Aligned Coulomb Tether Reconfiguration Analysis," *Journal of Astronautical Sciences*, Vol. 56, No. 4, Oct.–Dec. 2008, pp. 573–592.

[19] Natarajan, A., and Schaub, H., "Linear Dynamics and Stability Analysis of a Coulomb Tether Formation," *Journal of Guidance, Control, and Dynamics*, Vol. 29, No. 4, 2006, pp. 831–839. doi:10.2514/1.16480

[20] Natarajan, A., and Schaub, H., "Hybrid Control of Orbit Normal and Along-Track Two-Craft Coulomb Tethers," *Aerospace Science and Technology*, Vol. 13, Nos. 4–5, 2009, pp. 183–191. doi:10.1016/j.ast.2008.10.002

[21] Wang, S., and Schaub, H., "Coulomb Control of Nonequilibrium Fixed Shape Triangular Three-Vehicle Cluster," *Journal of Guidance, Control, and Dynamics*, Vol. 34, No. 1, 2011, pp. 259–270. doi:10.2514/1.47835

[22] Wang, S., and Schaub, H., "Nonlinear Charge Control for a Collinear Fixed Shape Three-Craft Equilibrium," *Journal of Guidance, Control, and Dynamics*, Vol. 34, No. 2, March–April 2011, pp. 359–366. doi:10.2514/1.52117

[23] Wang, S., and Schaub, H., "1-D Constrained Coulomb Structure Stabilization With Charge Saturation," *IEEE Transactions on Aerospace and Electronic Systems*, Vol. 48, No. 1, Jan. 2012, pp. 3–15. doi:10.1109/TAES.2012.6129617

[24] Saaj, C., Lappas, V. J., Schaub, H., and Izzo, D., "Hybrid Propulsion System for Formation Flying Using Electrostatic Forces," *Aerospace Science and Technology*, Vol. 14, No. 5, 2010, pp. 348–355. doi: 10.1016/j.ast.2010.02.009

[25] Pettazzi, L., Izzo, D., and Theil, S., "Swarm Navigation and Reconfiguration Using Electrostatic Forces," *Seventh International Conference on Dynamics and Control of Systems and Structures in Space*, Cranfield University Press, Cranfield, England, July 2006, pp. 257–267.

[26] DeForest, S. E., "Spacecraft Charging at Synchronous Orbit," *Journal of Geophysical Research*, Vol. 77, No. 4, 1972, pp. 651–659. doi:10.1029/JA077i004p00651

[27] Whipple, E. C., and Olsen, R. C., "Importance of Differential Charging for Controlling Both Natural and Induced Vehicle Potentials on ATS-5 and ATS-6," *Proceedings of the Third Spacecraft Charging Technology Conference*, NASA, Conference Publication 2182, 1980, p. 887.

[28] Eremenko, P., Brown, O., and Roberts, C., "Cost-Benefit Analysis of a Notional Fractionated SATCOM Architecture," *24th AIAA International Communications Satellite Systems Conference (ICSSC) and 4th Annual International Satellite & Communications (ISCe) Conference and Expo*, AIAA Paper 2006-5328, 2006.

[29] Schaub, H., and Moorer, D. F., "Geosynchronous Large Debris Reorbiter: Challenges and Prospects," *AAS Kyle T. Alfriend Astrodynamics Symposium*, American Astronautical Society Paper 10-311, 2010.

[30] Seubert, C. R., and Schaub, H., "Electrostatic Force Model for Terrestrial Experiments on the Coulomb Testbed," *61st International*

Astronautical Congress, Prague, CZ, International Astronautical Federation Paper 10.C1.1.9, Sept. 2010.

[31] Jasper, L. E. Z., and Schaub, H., "Effective Sphere Modeling for Electrostatic Forces on a Three-Dimensional Spacecraft Shape," *AAS/AIAA Spaceflight Mechanics Meeting*, Girdwood, Alaska, AAS Paper 11-465, 31 July–4 Aug. 2011.

[32] Sliško, J., and Brito-Orta, R. A., "On Approximate Formulas for the Electrostatic Force Between Two Conducting Spheres," *American Journal of Physics*, Vol. 66, No. 4, 1998, pp. 352–355. doi:10.1119/1.18864

[33] Soules, J. A., "Precise Calculation of the Electrostatic Force Between Charged Spheres Including Induction Effects," *American Journal of Physics*, Vol. 58, No. 12, 1990, pp. 1195–1199. doi:10.1119/1.16251

[34] Hogan, E., and Schaub, H., "Space Debris Reorbiting Using Electrostatic Actuation," *AAS Guidance and Control Conference*, Breckenridge, CO, AAS Paper 12-016, 3–8 Feb. 2012

[35] Denton, M. H., Thomsen, M. F., Korth, H., Lynch, S., Zhang, J. C., and Liemohn, M. W., "Bulk Plasma Properties at Geosynchronous Orbit," *Journal of Geophysical Research*, Vol. 110, No. A7, 2005. p. 17. doi:10.1029/2004JA010861

[36] Gurnett, D. A., and A., B., *Introduction to Plasma Physics — with Space and Laboratory Applications*, Cambridge Univ. Press, New York, 2005, pp. 8–9.

[37] Whipple, E. C., "Potentials on Surfaces in Space," *Reports on Progress in Physics*, Vol. 44, No. 11, 1981, pp. 1197–1250. doi:10.1088/0034-4885/44/11/002

[38] Murdoch, N., Izzo, D., Bombardelli, C., Carnelli, I., Hilgers, A., and Rodgers, D., "The Electrostatic Tractor for Asteroid Deflection," *58th International Astronautical Congress*, International Astronautical Federation Paper 08-A3.I.5, 2008.

[39] Schaub, H., and Junkins, J. L., *Analytical Mechanics of Space Systems*, 2nd ed., AIAA Education Series, AIAA, Reston, VA, Oct. 2009, Chap. 12.

[40] Battin, R. H., *An Introduction to the Mathematics and Methods of Astrodynamics*, AIAA Education Series, AIAA, New York, 1987, Chap. 10.